applied sciences

MDPI

Article

Design and Characterization of VHF Band Small Antenna Using CRLH Transmission Line and Non-Foster Matching Circuit

Soyeong Lee [1,†], Jonghyup Lee [2,†], Seongro Choi [3,†], Yong-Hyeok Lee [4], Jae-Young Chung [5], Keum Cheol Hwang [6] and Yong Bae Park [1,7,*]

[1] Department of AI Convergence Network, Ajou University, Suwon 16499, Korea; thdud723@ajou.ac.kr
[2] Korea Shipbuilding & Offshore Engineering, Seongnam 13591, Korea; jonghyup.lee@ksoe.co.kr
[3] DANAM Systems R&D Center, Anyang 13930, Korea; srchoi@danam.co.kr
[4] Microwave Technologies Group, Daejeon 34068, Korea; leeyh9612@mtginc.co.kr
[5] Department of Electrical and Information Engineering, Seoul National University of Science and Technology, Seoul 01811, Korea; jychung@seoultech.ac.kr
[6] School of Electronic and Electrical Engineering, Sungkyunkwan University, Suwon 16419, Korea; khwang@skku.edu
[7] Department of Electrical and Computer Engineering, Ajou University, Suwon 16499, Korea
* Correspondence: yong@ajou.ac.kr; Tel.: +82-31-219-2358
† These authors contributed equally to this work.

Received: 10 August 2020; Accepted: 10 September 2020; Published: 12 September 2020

Abstract: In this paper, we propose an electrically small antenna consisting of a composite right/left-handed (CRLH) transmission line (TL) and a non-Foster matching circuit. An interdigital capacitor (IDC) and spiral inductor are used to fabricate the very high frequency (VHF) band antenna based on CRLH TL. The size of the proposed antenna is as small as $0.025 \times 0.014 \times 0.0008\ \lambda$ at 145.5 MHz using the zeroth-order resonant generated by the CRLH TL. The antenna operation bandwidth is extended by the non-Foster circuit (NFC) consisting of a pair of transistors in a cross-coupled manner. An antenna prototype is fabricated and the input impedance, the received power, and gain of the proposed antenna are measured. The results show that the broadband characteristic is maintained while the form factor is extremely small compared to the wavelength. The average received power enhancement and increased bandwidth of antenna are 17.3 dB and 335.5 MHz (from 249.2–268.2 to 145.5–500 MHz), respectively. The calculated gain of the proposed antenna with the non-Foster is about −45 dBi at 155 MHz. The proposed antenna can be considered as a potential candidate of a low-profile antenna for military ground communications at the VHF band.

Keywords: composite right/left-handed transmission lines; military antenna; non-foster circuit; VHF band antenna

1. Introduction

For the military very high frequency (VHF) ground communication system, a conventional monopole or dipole antenna is mainly used. It guarantees reasonable gain for reliable wireless communications despite its long length (e.g., 0.5–5 m at VHF band) since the physical size of the antenna is proportional to the wavelength. This limits mobility and installation freedom on a platform. To overcome this, several small VHF band antennas have been proposed [1,2], but they are mostly not suitable for conformal installation or have inevitable limitation in an operation bandwidth.

Meanwhile, there have been many studies on the miniaturization of antennas using the composite right/left-handed (CRLH) transmission line (TL) technique [3–14]. CRLH TL is one of the metamaterial-inspired electromagnetic structures which is a composition of right- and left-handed TLs. By combining these two structures, the CRLH TL has the left-handed (LH) characteristics at a lower frequency and the right-handed (RH) characteristics at a higher frequency where the center frequency can be adjusted by the inductance and capacitance of the unit cell of CRLH TL. The LH characteristic provides a negative phase velocity which has an opposite wave propagating direction from the RH one, which is different from natural characteristic. The small antennas using the CRLH TL have been investigated mainly in the ultra-high frequency (UHF) band or higher bands. Recently, we proposed a VHF band small antenna using the CRLH TL in [9].

Although the CRLH TL can miniaturize the antenna physical size, the operation bandwidth is generally narrow due to its resonating nature. To improve the bandwidth, a non-Foster circuit (NFC) can be used as an impedance matching circuit [15–19]. However, the non-Foster circuits have not been used for the matching of the small VHF antennas using the CRLH TL. The non-Foster circuit generates a negative capacitance; therefore, it is useful to cancel the high positive capacitance of the antenna over a broad bandwidth.

In this paper, we applied a non-Foster circuit to the CRLH TL-based VHF antenna to resolve issues by the miniaturization such as bandwidth narrowing and receive power mitigation. The CRLH TL-based VHF antenna combined with the non-Foster matching circuit was designed using a full-wave electromagnetic simulator and radio frequency (RF) circuit simulator. We miniaturized the antenna with the zeroth-order resonant characteristic of the CRLH TL, and we obtained a wide bandwidth of the antenna using non-Foster impedance matching. The optimized antenna and circuit were fabricated, and then their individual characteristics as well as the combined antenna system characteristics were evaluated. The proposed 3-cell CRLH TL antenna consisted of interdigital capacitors and shunt spiral inductors to maximize the miniaturization effect. The size of the antenna was extremely small, $0.025 \times 0.014 \times 0.0008\ \lambda$ ($51.4 \times 30 \times 1.6$ mm), at the minimum operation frequency of the proposed antenna (145.5 MHz). Meanwhile, the size of the non-Foster circuit was only $0.0093 \times 0.006 \times 0.0007\ \lambda$ ($20 \times 14.4 \times 1.6$ mm). The measured 10-dB return loss bandwidth of the proposed antenna system was 145.5–500 MHz (354.5 MHz), which is 18 times wider than the CRLH TL antenna without the non-Foster circuit applied. The received power was also measured outdoors and an average of 17.3-dB enhancement was displayed in the frequency range of 120–500 MHz.

2. Design of Non-Foster Circuit

Unlike conventional circuits, non-Foster circuits generate negative impedance. All-natural impedance follows the Foster's reactance theorem. According to Foster reactance theorem, passive elements with a single port increase reactance as frequency increases [20]. Particularly, in the case of a passive element having a large impedance variation according to a frequency or in the case of a small antenna, the impedance of the antenna is matched in a very narrow bandwidth when using a conventional passive element such as an LC. Unlike the impedance matching method using a passive element, such as the conventional LC matching, the non-Foster circuit can reverse the reactance and reactance slope of a passive element to be matched; therefore, impedance matching can be performed over a wider band than originally. Figure 1 shows Foster impedance matching, which is a narrow band impedance matching, and Figure 2 shows non-Foster impedance matching, which is a wide band impedance matching. The non-Foster circuits are largely classified into two types: The circuit using an op-amps and the circuit using transistors [21]. The two methods differ in the active elements used; however, they are all impedance converter. Each circuit has advantages and disadvantages in design complexity and bandwidth. In this paper, a non-Foster circuit using transistors is designed for matching in a wide band over 50 MHz. The non-Foster circuit is designed by cross-coupled-junction transistors. In the case of a cross-coupled circuit, the phase of the input current is output same, but the phase of the input voltage is output 180° apart from each other. Because of this characteristic, the input impedance is inverted and becomes negative value. The non-Foster circuit can have any negative impedance value by inverting the impedance value of the passive element by connecting the passive element of the desired value to the circuit [22]. Figure 3 shows an equivalent circuit of a designed non-Foster circuit to increase the bandwidth of a CRLH TL antenna. In this paper, we designed a non-Foster circuit that satisfies the open circuit stable condition to connect the designed CRLH TL antenna in series. The gate and drain of the two transistors were cross-coupled. To optimize the non-Foster circuit element values, we used the Agilent ADS2009 circuit simulator. We used the Avago ATF-53189 transistor with an operating frequency of 50 MHz to 6.5 GHz to consider the transistor's internal parasitic effects and obtain broadband characteristic of the non-Foster circuit [23]. Table 1 shows the parameters of the designed non-Foster circuit.

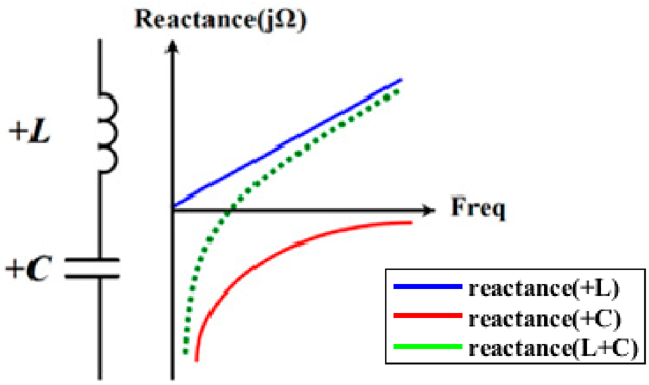

Figure 1. Foster impedance matching.

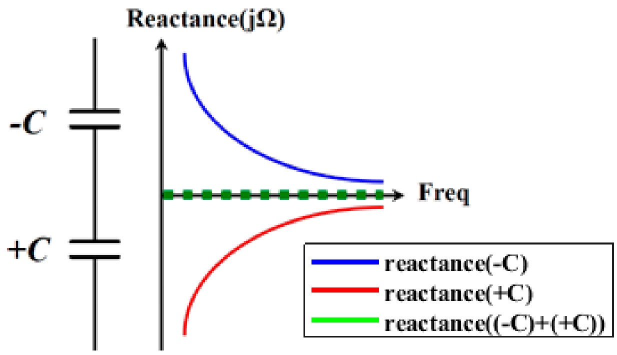

Figure 2. Non-Foster impedance matching.

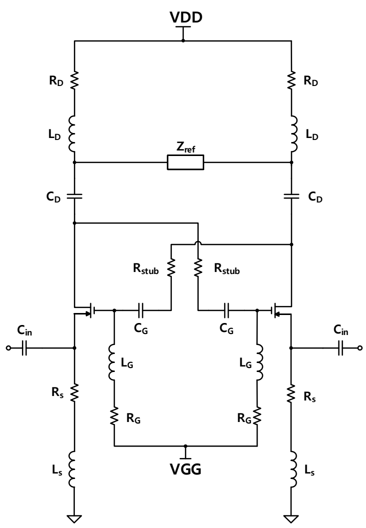

Figure 3. Schematic of non-Foster circuit.

Table 1. Parameters of the non-Foster circuit.

Parameters	Value
Z_{ref}	7 pF
L_G	0.47 uH
L_D	0.47 uH
L_S	0.47 uH
R_G	1.5 kΩ
R_D	1.5 kΩ
R_S	1.5 kΩ
R_{stab}	51 Ω
C_{stab}	1 pF
C_G	510 pF
C_D	510 pF
C_{in}	100 pF

It is well known that a non-Foster circuit may exhibit instability due to the positive feedback formed in the transistor-ground loop. Therefore, it is important to verify stability in the non-Foster circuit design [24]. In this paper, we verified stability with two methods: by checking impedance of the non-Foster circuit and the transient response in the time domain. Figure 4 shows the impedance of the non-Foster circuit and load. In order to satisfy the open circuit stable condition, the impedance of the non-Foster circuit should be smaller than the impedance of the load [25] (i.e., $Z_{Load} > Z_{NFC}$). Both the simulated and measured results show that the proposed non-Foster circuit satisfies the open circuit stable condition throughout the observation frequency range. The differences between the simulation and measurement values originated from the difference between the ideal environment and the real one. The latter includes the effects from lossy and reactive parasitic components. Figure 5 shows the impedance measurement environment.

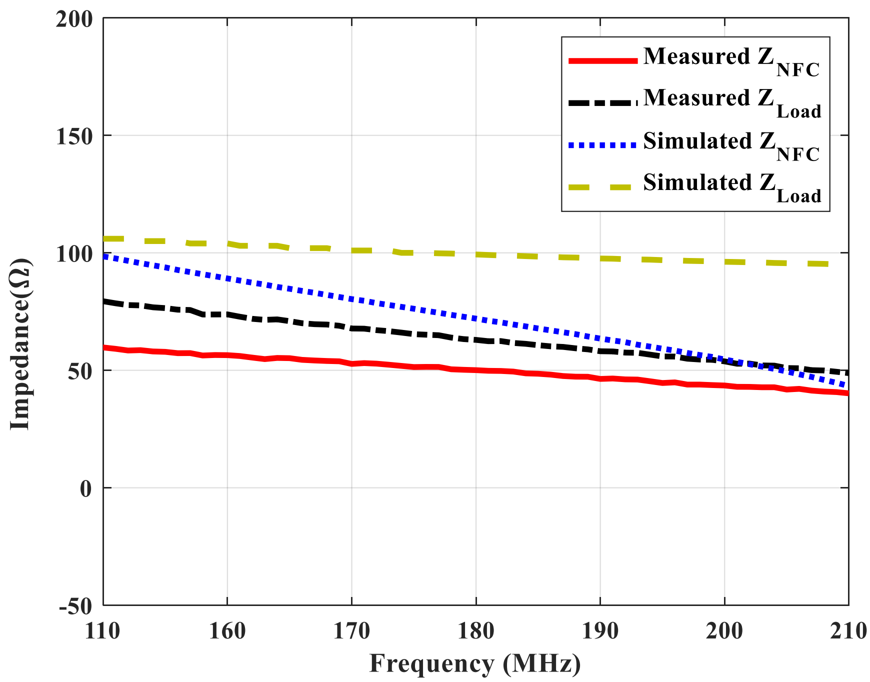

Figure 4. The simulated and measured impedance values of load and non-Foster circuit.

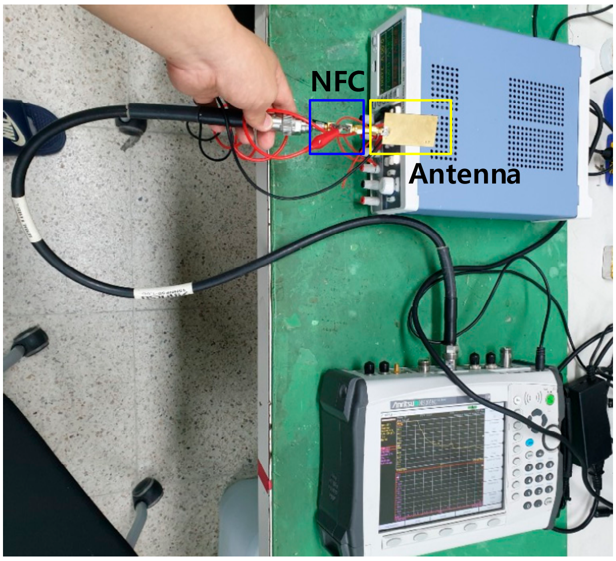

Figure 5. Impedance measurement environment.

Figure 6 shows transient response of the non-Foster circuit which oscillated at the beginning but damped as the time pass. This represents that the circuit was stable. The open circuit stable condition discussed in the previous paragraph was valid for an ideal dispersionless circuit, but no circuit is dispersionless in the real world. Unwanted small oscillations due to parasitic components and imperfections in transmission lines may have diverged as the currents traveled through the non-Foster circuit's feedback loop. Thus, we also looked into the transient response as other researchers have [25]. If either the R, L, or C component of the circuit combined to the load had a negative value, the time constant became negative, which implied that the thermal noise voltage or current exponentially increased with the passage of time. As the result, the non-Foster circuit would oscillate at a certain frequency and would be unstable. Ideally, an impulse with infinite bandwidth should be used to check the stability. However, using a pulse with a broad enough bandwidth afforded valid results for the stability check since the employed transistor had limited bandwidth providing the gain. In our case, we generated a pulse based on the white Gaussian noise with the bandwidth covering the transistor's operating bandwidth, and then checked whether the transient response was damping as in Figure 6. For the case where the open circuit stable condition was met but the transient response was diverging, the bias voltages and RLC components were tuned to satisfy both conditions. The validity was assessed by the simulation and measurement.

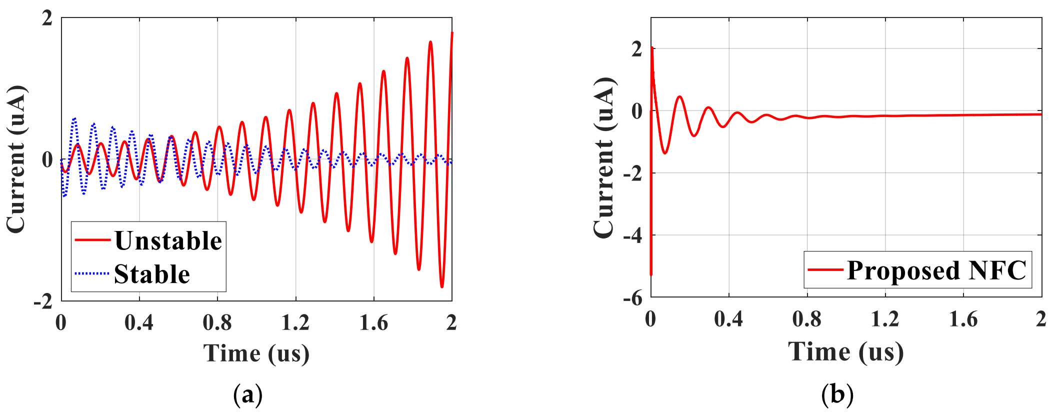

Figure 6. The transient response of non-Foster circuits: (**a**) Examples of stable and unstable transient responses; (**b**) the transient response of the proposed non-Foster circuit.

3. Design of CRLH Transmission Line Antenna

In our previous work [9], we proposed a CRLH TL-based VHF antenna with operating-frequencies from 159.6 to 164.4 MHz. In this paper, we designed and optimized another CRLH TL-based VHF antenna with the operating frequencies from 249.2–268.2 MHz. Figure 7 illustrates an equivalent circuit of a general CRLH TL unit cell, which is decomposed into a left-handed circuit and right-handed one. The left-handed circuit technically consists of a series capacitance (C_L) and a shunt inductance (L_L). However, it should be noted that the pure LH circuit does not exist because of the properties of the transmission line, i.e., the parasitic series inductance (L_R) and the shunt capacitance (C_R). The parasitic capacitance is induced due to voltage gradients between the metal patterns and the ground plane. In CRLH TL, a magnetic field occurs when a current flows along a series capacitance [26]. CRLH TL has a zeroth-order resonant frequency in which the propagation number becomes zero. Below the zeroth-order resonant frequency, CRLH TL has LH TL characteristics and above zeroth-order resonant frequency, CRLH TL has RH TL characteristics.

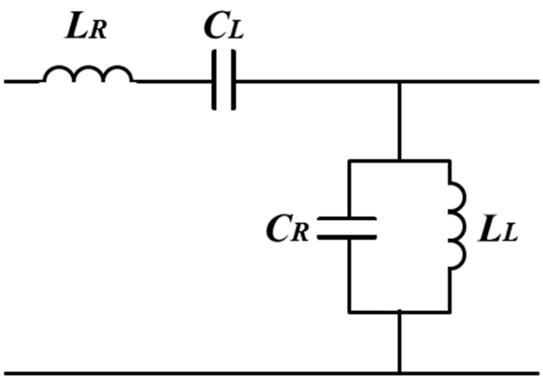

Figure 7. Equivalent circuit of composite right/left-handed (CRLH) transmission line.

At the zeroth-order frequency, the resonant frequency is independent from physical size of the antenna, so the antenna can be miniaturized. The zeroth-order resonant frequency is determined by the shunt resonant frequency in the case of open termination [26].

$$\omega_{sh} = \frac{1}{\sqrt{C_R L_L}} \tag{1}$$

By Equation (1), the zeroth-order resonant frequency can be adjusted by shunt capacitance and inductors, which means that the zeroth-order frequency can be adjusted by the unit cell parameter of CRLH TL. Figure 8 shows the design procedure for CRLH TL antenna. First, we designed a basic model of a CRLH TL unit cell. We optimized the zeroth-order resonant frequency to target frequency with optimizing parameters of the CRLH TL unit cell. After optimization, we arranged three CRLH TL unit cells to obtain CRLH TL characteristics. To enhance CRLH TL characteristics, CRLH TL had to have more than two unit cells [26]. It should be noted that the input impedance of CRLH TL was changed when the unit cells were arranged. Because of this characteristic, we matched the input impedance of the CRLH TL.

Figure 9 shows a unit cell of the designed CRLH TL. We implemented an interdigital capacitor (IDC) to realize series capacitance (C_L). Using IDC, we could obtain large capacitance by adjusting the number of fingers and parameters of the IDC and implementing series capacitance. In addition, we implemented a spiral inductor which was connected to the ground to realize shunt inductance (L_L). Using the spiral inductor, we could obtain large inductance while minimizing the inductor area. The C_L and the L_L were artificially implemented with a designing structure, and then the values of C_L and L_L were adjusted by changing the parameters of the unit cell. The extracted parameters of the CRLH TL unit cell using a pseudo-inverse technique are shown in Table 2 [27]. In the simulation, the zero-order resonance frequency was designed at the desired frequency by optimization of the unit cell parameter. Figure 10 shows a 3D view of the CRLH TL unit cell. In this paper, we used FR-4 substrate. The relative dielectric constant of the substrate was 4.4 with the thickness of h = 1.6 mm. Table 3 shows the parameters of the optimized unit cell and Figure 11 shows the designed CRLH TL antenna. To realize CRLH TL characteristics, CRLH TL consisted of at least 2 unit cells. In this paper, the antenna consisted of 3 unit cells.

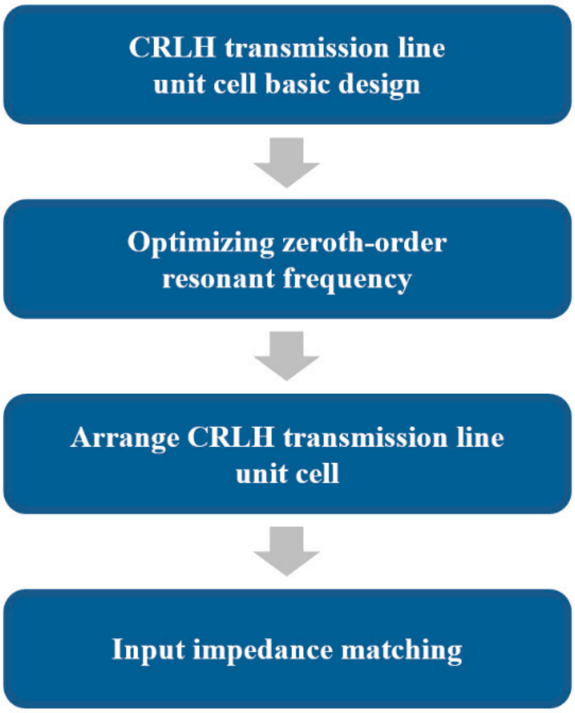

Figure 8. Design procedure for CRLH transmission line antenna.

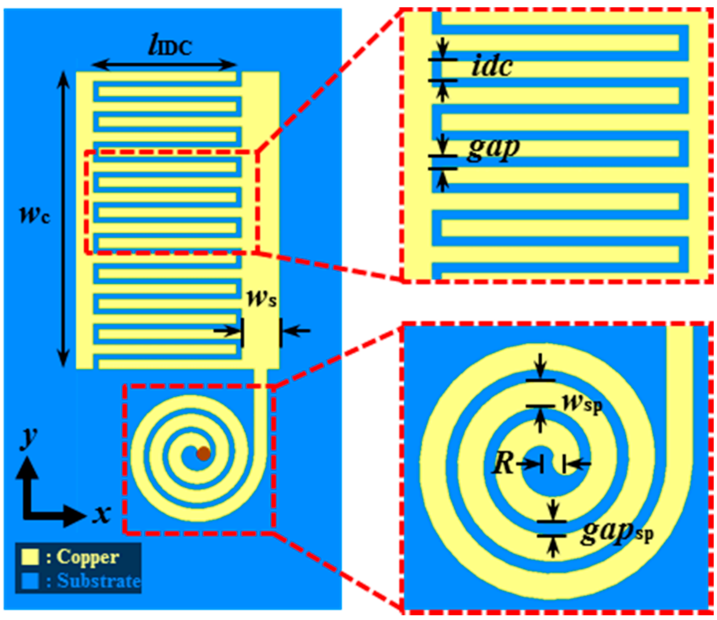

Figure 9. CRLH transmission line unit cell.

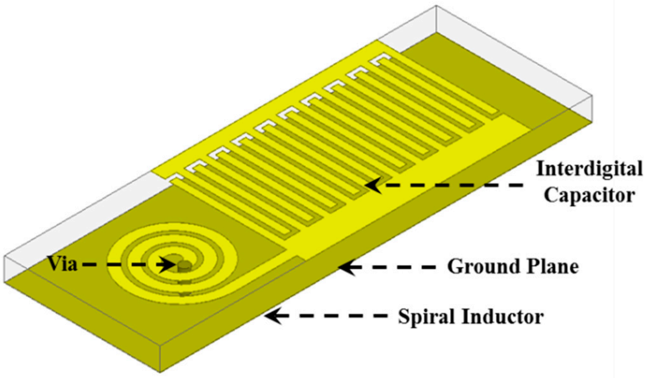

Figure 10. 3D view of the CRLH transmission line unit cell.

Table 2. Parameters of the CRLH TL unit cell.

Parameters	Value
C_R	7.382 pF
L_L	19.955 nH
C_L	4.177 pF
L_R	1.013 nH

Table 3. Parameters of the CRLH TL unit cell.

Parameters	Value
w_c	15.7
w_s	2
l_{IDC}	7.5
idc	0.5
gap	0.3
w_{sp}	0.7
R	0.5
gap_{sp}	1
w_c	15.7
w_s	2

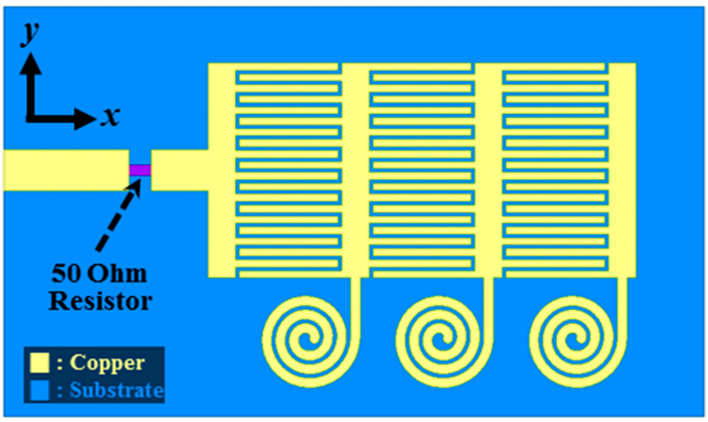

Figure 11. Designed CRLH transmission line antenna.

The size of the antenna was 0.025 × 0.014 × 0.0008 λ (51.4 × 30 × 1.6 mm). Because the input impedance of the antenna should be close to about 30–70 Ω for the impedance matching between the antenna and the non-Foster circuit, a 50-Ω chip resistor was implemented to the antenna feeding part. As the frequency of the CRLH TL antenna decreased, the input reactance became negative due to the series capacitance. The non-Foster circuit could broaden the antenna operating bandwidth by canceling the negative input reactance of the antenna by generating negative capacitance. Since the non-Foster had a constant negative capacitance across the target operating bandwidth, the input resistance of the antenna had to be maintained at about 30 to 70 Ω over the target frequency band, and the slope of the antenna input reactance value, i.e., the capacitance, had to be kept constant. The capacitance of the antenna is approximated by the following equation.

$$\mathrm{Imag}\,(Z_{in}) = \frac{1}{j\omega C}\quad (\mathrm{C} = \mathrm{capacitance}) \tag{2}$$

Equation (2) is converted to Equation (3).

$$C = \frac{1}{j\omega \mathrm{Imag}\,(Z_{in})} \tag{3}$$

Figure 12 shows the input impedance of the CRLH TL antenna. Figure 13 shows the simulated radiation patterns on the Y–Z (E-Plane) and X–Z (H-Plane) planes at 155 MHz. Table 4 shows the antenna capacitance versus frequency. It was confirmed that a constant capacitance of 9 to 12 pF was obtained at 126–186 MHz.

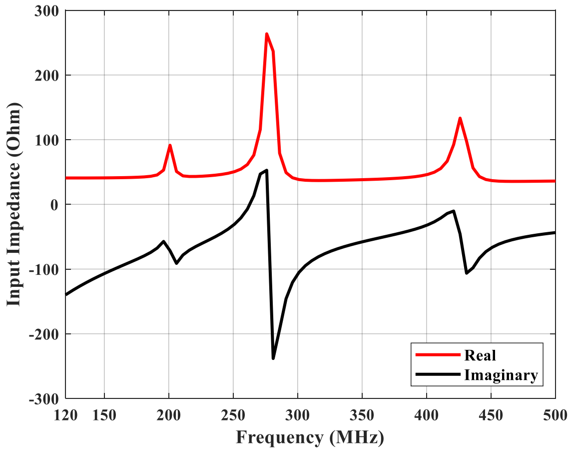

Figure 12. Input impedance of CRLH transmission line antenna.

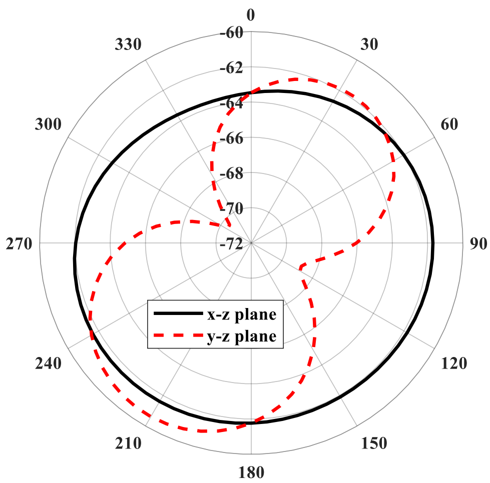

Figure 13. Simulated radiation patterns of the antenna.

Table 4. Capacitance of the antenna versus frequency.

Frequency (MHz)	Capacitance (pF)
126	9.55
131	9.61
136	9.68
141	9.76
146	9.84
151	9.94
156	10.05
161	10.18
166	10.33
171	10.51
176	10.75
181	11.06
186	11.52
191	12.32
196	14.15

4. Measurement

Figure 14 shows the CRLH TL antenna combined with the non-Foster circuit. An SMA connector was used for connecting the CRLH TL antenna and non-Foster circuit. Figure 15 shows the received power measurement environment. Alaris's OMNI-A0245 antenna was used for a transmitting antenna. The gain of the transmitting antenna was from −7 to −3 dBi at 120–500 MHz [28]. One mW power was applied to the transmitting antenna. The distance between the transmitting antenna and receiving antenna was 10 m, above four times that of the wavelength (2.06 m) of the minimum operating frequency (145.5 MHz) to meet the far-field conditions.

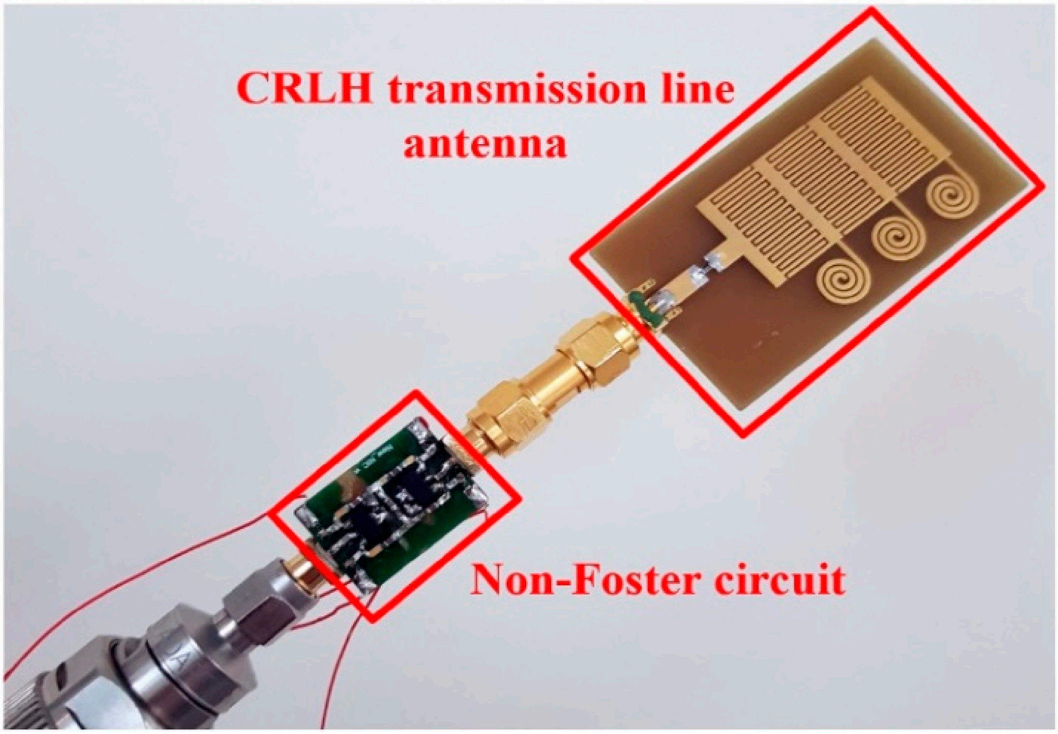

Figure 14. Designed CRLH transmission line antenna.

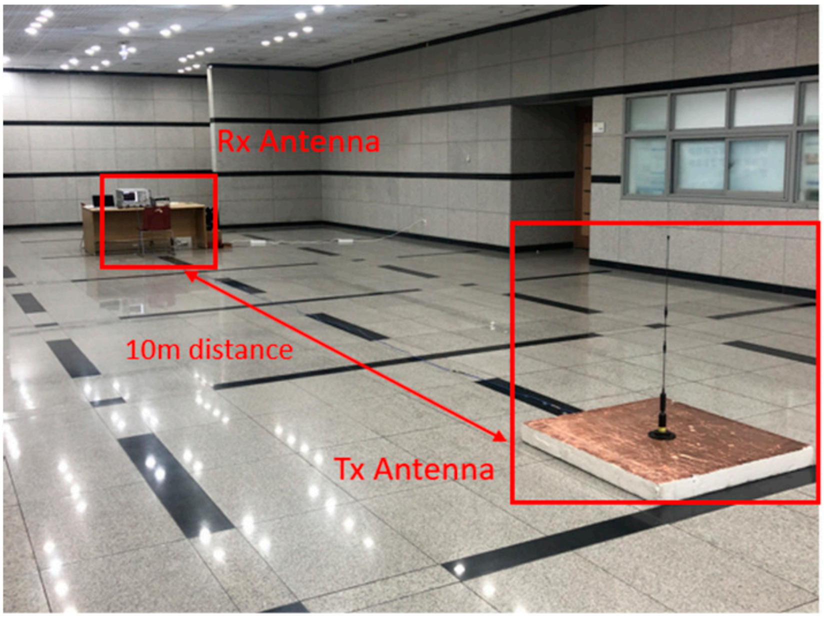

Figure 15. Received power measurement environment.

Figure 16 shows the measured reflection coefficient of the proposed antenna with and without the non-Foster. It shows that the CRLH TL antenna without the non-Foster circuit did not resonate in the military VHF band. However, the CRLH TL antenna with the non-Foster circuit showed a reflection coefficient less than −10 dB in 145.5–500 MHz due to the impedance matching by the non-Foster circuit. The operating frequencies of the proposed antenna included the military VHF band. In order to investigate the loss due to the non-Foster circuit, the input impedance of the non-Foster circuit was measured as in Figure 17. The real part indicated the loss, showing that it ranged between 11–16 ohm which implied the loss originated from the non-Foster circuit itself was non-negligible. The imaginary part showed a traditional negative slope as the frequency increases (i.e., j/ωc). We note that the reflection coefficient of the non-Foster circuit itself was high since the impedance had a big difference from the port impedance of the vector network analyzer, which was 50 + j0 ohm.

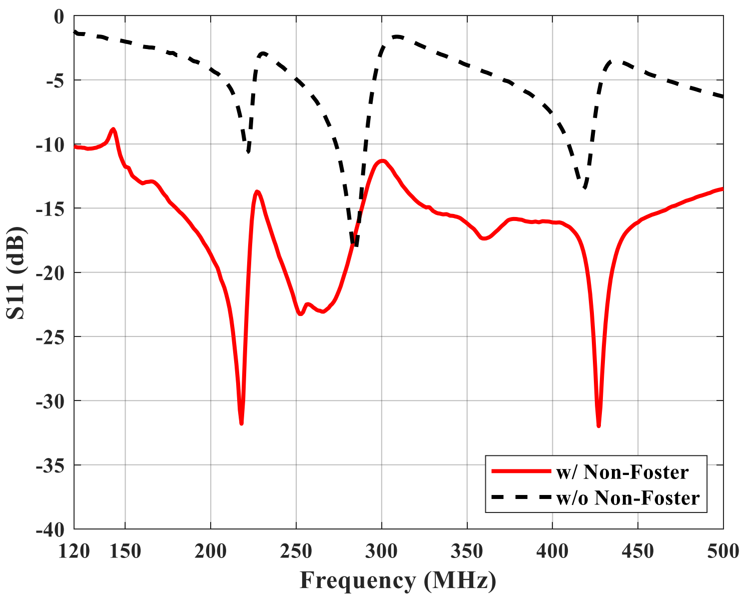

Figure 16. Measured reflection coefficients.

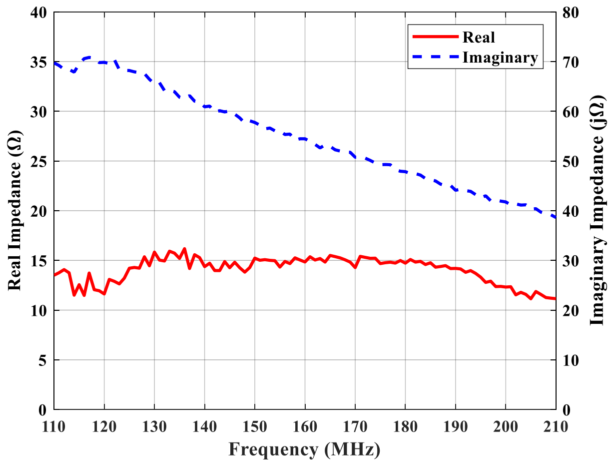

Figure 17. The measured impedance of the non-Foster circuit.

Figure 18 shows the received power of the antenna. Since the non-Foster circuit was used to match the input impedance of the antenna, the received power was enhanced. Comparing the received power before and after applying the non-Foster circuit, the received power enhancement ratio was 17.3 dB on an average of 120 to 500 MHz. Figure 19 shows the proposed antenna gain calculated by Friis' transmission formula. The formula of Friis' transmission is as follows.

$$P_r = G_t G_r P_t \left(\frac{\lambda}{4\pi r}\right)^2 \tag{4}$$

Equation (4) can be used to calculate the gain of the receiving antenna from the received power.

$$G_r = \frac{P_r}{G_t P_t} \left(\frac{4\pi r}{\lambda}\right)^2 \tag{5}$$

By Equation (5), we can calculate the gain of the proposed antenna. The comparison between the simulated gain of the proposed antenna and the measured gain showed a similar tendency. It is worth noting that experimental results showed the non-Foster circuit became unstable as the power was increased. Thus, the proposed antenna was not suitable for the transmitting side, but the receiving side [29].

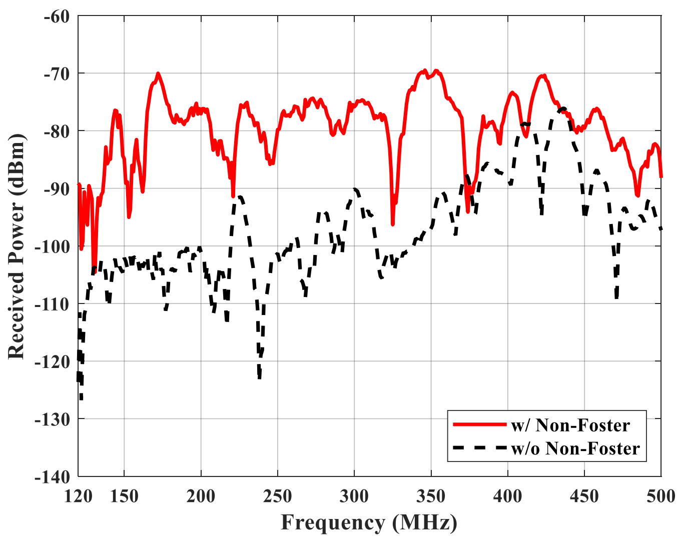

Figure 18. Measured received powers.

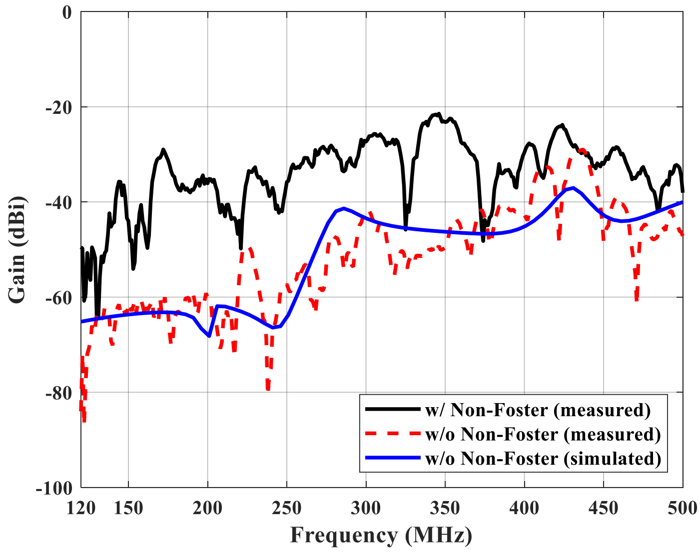

Figure 19. Measured and simulated gain of the antenna (note: "w/o Non-Foster" indicates the antenna was matched using ordinary passive matching technique).

Table 5 shows the comparison of our antenna with other CRLH TL antennas. Note that the bandwidth of our antenna was more or less than that of other antennas, but only our antenna was implemented in the VHF band using CRLH TL with the non-Foster matching circuit.

Table 5. Comparison table with CRLH antennas.

Reference	Antenna Size	Bandwidth	Substrate
2015 [10]	$22 \times 30 \times 0.8$ mm^3 $0.21\lambda_0 \times 0.29\lambda_0 \times 0.008\lambda_0$ @2.9 GHz	4 GHz (2.6–6.6 GHz) 87%	Duroid 5880
2015 [11]	$20.4 \times 6.8 \times 0.8$ mm^3 $0.39\lambda_0 \times 0.13\lambda_0 \times 0.015\lambda_0$ @5.8 GHz	1.5 GHz (5.8–7.3 GHz) 23%	RO4003
2017 [12]	$21.5 \times 30 \times 0.8$ mm^3 $0.372\lambda_0 \times 0.52\lambda_0 \times 0.014\lambda_0$ @5.2 GHz	6.8 GHz (1.8–8.6 GHz) 120%	RO4003
2018 [13]	$23 \times 17 \times 1.6$ mm^3 $0.037\lambda_0 \times 0.027\lambda_0 \times 0.0026\lambda_0$ @0.48 GHz	6.02 GHz (0.48–6.5 GHz) 172.49%	Duroid 5880
2018 [14]	$17.5 \times 32.15 \times 1.6$ mm^3 $0.204\lambda_0 \times 0.375\lambda_0 \times 0.018\lambda_0$ @3.5 GHz	7.05 GHz (0.85–7.9 GHz) 161.14%	FR-4
proposed antenna	$31.4 \times 23.7 \times 1.6$ mm^3 $0.014\lambda_0 \times 0.01\lambda_0 \times 0.0007\lambda_0$ @0.14 GHz	0.153GHz (0.14–293 GHz) 70.3%	FR-4

5. Conclusions

An electrically small antenna consisting of a composite right/left-handed transmission line and a non-Foster matching circuit was proposed. In order to manufacture an electrically small antenna, a unit cell composed of an IDC and spiral inductor was designed. The CRLH TL antenna was fabricated by connecting three unit cells to obtain CRLH characteristics. The size of the proposed antenna was as small as 0.025 $\lambda \times 0.014\ \lambda \times 0.0008\ \lambda$ at 145.5 MHz using the zeroth-order resonant generated by the CRLH transmission line. The non-Foster circuit that could generate negative capacitance was designed by cross-coupled-junction transistors. By checking the load impedance and the transient response in the time domain, we confirmed the stability of the non-Foster matching circuit. By using the non-Foster matching circuit in the CRLH antenna, the bandwidth was increased by 335.5 MHz and the average received power was enhanced by 17.3 dB. In addition, the calculated gain using Friis' transmission formula at our target frequency was increased by more than 15 dBi. We note that the received power and gain improvements were measured and evaluated instead of the absolute gain and radiation efficiency due to the limitations of the measurement facility at the VHF band. Nevertheless, the improvements by applying the non-Foster circuit were clearly demonstrated using these relative parameters. The proposed antenna system can be considered as a potential candidate of a low-profile receiving antenna for military ground communications at the VHF band.

Author Contributions: The present work was conducted in cooperation with all authors. S.L., J.L. and S.C. analyzed the problem and performed numerous simulations; S.L., J.L., S.C., Y.-H.L., J.-Y.C., K.C.H. and Y.B.P. contributed to the conceptualization, fabrication, and measurement; S.L., J.L. and S.C. wrote a draft which was edited by all co-authors. All authors have read and agreed to the published version of the manuscript.

Funding: This research received no external funding.

Acknowledgments: This work has been supported by the Future Combat System Network Technology Research Center program of Defense Acquisition Program Administration and Agency for Defense Development. (UD190033ED).

Conflicts of Interest: The authors declare no conflict of interest.

References

1. Hascall-Denke. Manpack Antenna Products Book. Available online: http://www.hascall-denke.com/product-lines/military-antennas/manpack-antennas/ (accessed on 3 June 2019).
2. Hascall-Denke. Vehicular/Marine Antenna Products Book. Available online: http://www.hascall-denke.com/product-lines/military-antennas/marine-antennas/ (accessed on 3 June 2019).
3. Lai, A.; Leong, K.M.; Itoh, T. Infinite wavelength resonant antennas with monopolar radiation pattern based on periodic structures. *IEEE Trans. Antennas Propag.* **2007**, *55*, 868–876. [CrossRef]
4. Qureshi, F.; Antoniades, M.A.; Eleftheriades, G.V. A compact and low-profile metamaterial ring antenna with vertical polarization. *IEEE Antennas Wirel. Propag. Lett.* **2005**, *4*, 333–336. [CrossRef]
5. Jang, T.; Choi, J.; Lim, S. Compact coplanar waveguide (CPW)-fed zeroth-order resonant antennas with extended bandwidth and high efficiency on vialess single layer. *IEEE Trans. Antennas Propag.* **2010**, *59*, 363–372. [CrossRef]
6. Ha, J.; Kwon, K.; Choi, J. Compact Zeroth-order Resonance Antenna for Im-plantable Biomedical Service Application. *Electron. Lett.* **2011**, *47*, 1267–1269. [CrossRef]
7. Kim, S.; Lee, J. Frequency and Bandwidth of the Negative/Positive nth Mode of a Composite Right-/Left-Handed Transmission Line. *J. Electromagn. Eng. Sci.* **2018**, *18*, 1–6. [CrossRef]
8. Nelaturi, S.; Sarma, N. A Compact Microstrip Patch Antenna Based on Metamaterials for WiFi and WiMAX Application. *J. Electromagn. Eng. Sci.* **2018**, *18*, 182–187. [CrossRef]
9. Jun, H.J.; Lee, J.; Choi, S.; Park, Y.B. Design and Fabrication of VHF Band Small Antenna Using Composite Right/Left-Handed Transmission Lines. *J. Electr. Eng. Technol.* **2019**, *14*, 339–345. [CrossRef]
10. Alibakhshi-Kenari, M.; Naser-Moghadasi, M.; Sadeghzadeh, R.A. Bandwidth and Radiation Specifications Enhancement of Monopole Antennas Loaded with Split Ring Resonators. *IET Microw. Antennas Propag.* **2015**, *9*, 1487–1496. [CrossRef]
11. Alibakhshi-Kenari, M.; Naser-Moghadasi, M.; Virdee, B.S.; Andújar, A.; Anguera, A. Compact Antenna based on a Composite Right/Left-Handed Transmission Line. *Microw. Opt. Technol. Lett.* **2015**, *57*, 1785–1788. [CrossRef]
12. Alibakhshi-Kenari, M.; Virdee, B.S.; Limiti, E. Compact Single Layer Travelling-Wave Antenna Design Using Metamaterial Transmission-Lines. *Radio Sci.* **2017**, *52*, 1510–1521. [CrossRef]
13. Alibakhshi-Kenari, M.; Virdee, B.S.; Ali, A.; Limiti, E. Miniaturized Planar-Patch Antenna Based on Metamaterial L-shaped Unit-Cells for Broadband Portable Microwave Devices and Multiband Wireless Communication Systems. *IET Microw. Antennas Propag.* **2018**, *12*, 1080–1086. [CrossRef]
14. Alibakhshi-Kenari, M.; Virdee, B.S.; Ali, A.; Limiti, E. Extended Aperture Miniature Antenna Based on CRLH Metamaterials for Wireless Communication Systems Operating Over UHF to C-Band. *Radio Sci.* **2018**, *53*, 154–165. [CrossRef]

15. Saadat, S.; Adnan, M.; Mosallaei, H.; Afshari, E. Composite Metamaterial and Metasurface Integrated with Non-Foster Active Circuit Elements: A Bandwidth-Enhancement Investigation. *IEEE Trans. Antennas Propag.* **2013**, *61*, 1210–1218. [CrossRef]
16. Sussman-Fort, S.E.; Rudish, R.M. Non-Foster impedance matching of electrically-small antennas. *IEEE Trans. Antennas Propag.* **2009**, *57*, 2230–2241. [CrossRef]
17. Go, J.-G.; Chung, J.-Y. Non-Foster Matching Circuit Design to Improve VHF and UHF-Band Small Antenna Impedance Matching. *J. Korean Inst. Electromagn. Eng. Sci.* **2018**, *29*, 159–166. [CrossRef]
18. Ha, S.; Cho, J.; Jung, K. Design of Miniaturized Microstrip Patch Antennas Using Non-Foster Circuits for Compact Controlled Reception Pattern Antenna Array. *J. Electromagn. Eng. Sci.* **2017**, *17*, 108–110. [CrossRef]
19. White, C.R.; Colburn, J.S.; Nagele, R.G. A non-Foster VHF monopole antenna. *IEEE Antennas Wirel. Propag. Lett.* **2012**, *11*, 584–587. [CrossRef]
20. Foster, R.M. A reactance theorem. *Bell Syst. Tech. J.* **1924**, *3*, 259–267. [CrossRef]
21. Long, J. Non-Foster Circuit Loaded Periodic Structures for Broadband Fast and Slow Wave Propagation. Ph.D. Thesis, University of California, San Diego, CA, USA, 2015.
22. Linvill, J.G. Transistor negative impedance converters. *Proc. IRE* **1953**, *41*, 725–729. [CrossRef]
23. Avago. E-pHEMT ATF-53189 Datasheet. 2013. Available online: https://docs.broadcom.com/doc/AV02-0051EN/ (accessed on 5 June 2019).
24. Song, K.S. Non-Foster Impedance Matching and Loading Networks for Electrically Small Antenna. Ph.D. Thesis, The Ohio State University, Columbus, OH, USA, 2011.
25. Jacob, M.M. Non-Foster Circuit for High Performance Antennas: Advantages and Practical Limitation. Ph.D. Thesis, University of California, San Diego, CA, USA, 2016.
26. Caloz, C.; Itoh, T. *Electromagnetic Metamaterials: Transmission Line Theory and Microwave Applications*; Wiley-IEEE Press: New York, NY, USA, 2005.
27. Kou, N.; Shi, Y.; Li, L. New Equivalent Circuiminiat Analysis and Synthesis for Broadband Composite Right/Left-Handed Transmission Line Metamaterials. *ACES J.* **2016**, *31*, 884–893.
28. Alaris, A. OMNI-A0245 Datasheet. Available online: https://www.Alarisantennas.com/products/passive-monitoring-antenna-2/ (accessed on 5 June 2019).
29. Picher, C.; Anguera, J.; Andújar, A.; Borja, C.; Puente, C.; Kahng, S. Reuse of the Mobile Communication Antenna for FM Reception. In Proceedings of the 5th European Conference on Antennas and Propagation (EUCAP), Rome, Italy, 11–15 April 2011; pp. 324–327.